Received: 9 December 2024 | Accepted: 19 January 2025

DOI: 10.1002/vzj2.70004

Vadose Zone Journal

ORIGINAL ARTICLE

Modeling compaction effects on soil water retention across the full moisture range: Calibration and validation

Andre Peters[1] | **Zhengchao Tian**[2] | **Joshua L. Heitman**[3] | **Sascha C. Iden**[4] | **Lennart Rolfes**[1] | **Kai Germer**[1] | **Marco Lorenz**[1]

[1]Thünen Institute of Agricultural Technology, Braunschweig, Germany

[2]College of Resources and Environment, Huazhong Agricultural University, Wuhan, P. R. China

[3]Crop and Soil Sciences Department, North Carolina State University, Raleigh, North Carolina, USA

[4]Division of Soil Science, Institute for Geoecology, Technische Universität Braunschweig, Braunschweig, Germany

Correspondence
Sascha C. Iden, Division of Soil Science, Institute for Geoecology, Technische Universität Braunschweig, Braunschweig, Germany.
Email: s.iden@tu-braunschweig.de

Assigned to Associate Editor Dianna Bagnall.

Funding information
BonaRes, Grant/Award Number: 031B1065A

Abstract

Soil compaction leads to an increase in bulk density (ρ_b) and results in a shift in pore-size distribution toward smaller pores. These changes alter the soil hydraulic properties (SHPs), that is, the water retention curve and the hydraulic conductivity curve. Most existing models that address the impact of changes in ρ_b on SHP have been confined to SHP models that consider only capillary water, neglecting water stored and transmitted within adsorbed films (noncapillary water). Recently, a new prediction model was developed that combines the Peters–Durner–Iden (PDI) SHP model system, which accounts for capillary and noncapillary water, with a prediction scheme for compaction effects. However, this new approach has yet to be calibrated and tested against data from soils with varying textures. The objective of this study was to calibrate and evaluate the new water retention model using a comprehensive dataset from the literature. Two different variants, which vary in the number of degrees of freedom have been tested. Remarkably, the variant with only one adjustable parameter, the one that shifts the pore-size distribution by scaling the pressure head, was sufficient to accurately describe the data. All other parameters can either be fixed at the reference value or scaled based on straightforward physical reasoning. The model achieved low calibration errors (median root mean square error [RMSE]: 0.013; median mean error [ME]: 0.0014) and performed satisfactorily in validation (median RMSE: 0.025; median ME: −0.014). Based on our results, we hypothesize that the scaling approach is independent of the capillary saturation function and that this method might be applied to other models within the PDI system without new calibration.

Plain Language Summary

Soil compaction increases soil density and shifts pores toward smaller sizes, affecting how soil stores and transmits water. Existing prediction models for compaction effects often overlook noncapillary water, which is stored in thin films on soil particles. A new model combines a comprehensive soil hydraulic property (SHP) model

with a method to predict compaction effects. This study tested the model using data from various soil types. Surprisingly, the version requiring just one adjustable parameter, scaling the pore-size distribution, accurately fit the data. Other parameters were either fixed or adjusted using simple physical rules. The model showed low errors in calibration and validation, demonstrating reliability. This approach can also be adapted to other SHP models without needing recalibration.

1 | INTRODUCTION

Soil compaction influences various soil properties, which in turn impact plant development and crop productivity (O'Sullivan & Simota, 1995). For instance, it increases the resistance encountered by roots as they grow, leading to shallower root systems and, in severe cases, stunted plant development and lower crop yields (Whalley et al., 1995). Consequently, preventing compaction can help stabilize or even increase yields and support sustainable agriculture (Duttmann et al., 2022; Horn, 2003; McPhee et al., 2020; Soane & van Ouwerkerk, 1994; Tullberg, 2010).

The influence of compaction on soil hydraulic properties (SHPs), namely, the water retention curve (WRC) and the hydraulic conductivity curve (HCC), has been investigated by many researchers (e.g., Allbrook, 1986; Bruand & Cousin, 1995; Gupta et al., 1989; Hill & Sumner, 1967). Compaction reduces the total porosity, shifts the pore-size distribution toward smaller pores, and increases the volumetric water contents in the hygroscopic moisture range (Assouline, 2006a; Peters et al., 2025; Tian et al., 2018).

A simple measure for soil compaction is the easy-to-measure bulk density (ρ_b [g cm^{-3}]). As stated above, changes in ρ_b and SHP are highly related. This has been accounted for in several empirical approaches to model the effect of changed bulk density on soil hydraulic functions (e.g., Assouline, 2006a, 2006b; Mualem & Assouline, 1989; Ngo-Cong et al., 2021; Tian et al., 2018, 2019).

The abovementioned approaches scale the parameters of hydraulic functions that account only for capillary effects, thereby neglecting noncapillary effects, such as water adsorption on mineral surfaces and film conductivity. The most commonly used model combination is the van Genuchten (1980) water retention function with the Mualem (1976) hydraulic conductivity model (van Genuchten, 1980). Furthermore, these approaches must be scaled by an observed or assumed value of saturated hydraulic conductivity since they predict the relative conductivity. The saturated hydraulic conductivity is highly uncertain, as it is strongly influenced by soil structure and biological pores (Usowicz & Lipiec, 2021). Hence, scaling the complete conductivity curve with this parameter can lead to a biased conductivity prediction in the complete moisture range (Peters, Hohenbrink, et al., 2023; Schaap & Leij, 2000).

The Peters–Durner–Iden (PDI) model system for describing SHPs incorporates water storage in capillaries and on particle surfaces (Iden & Durner, 2014; Peters, 2013, 2014). Recently, it was updated with a scheme that enables the

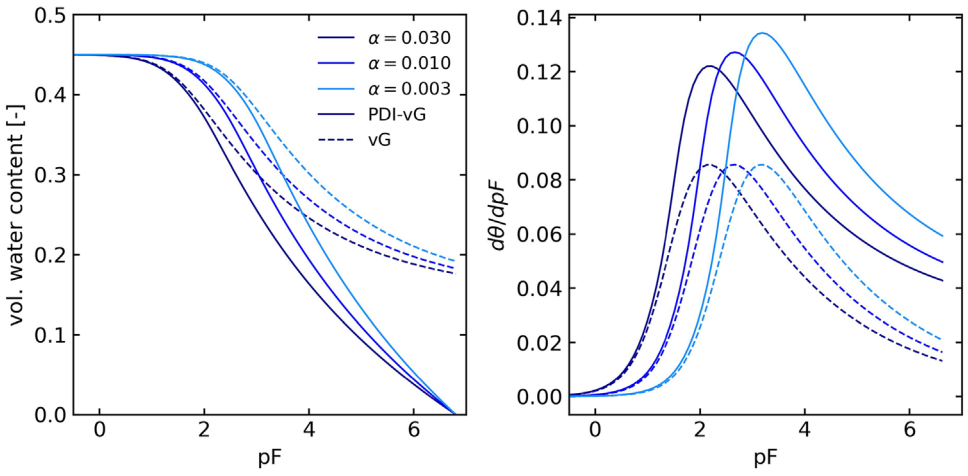

FIGURE 1 Influence of scaling α on pore-size distribution for the van Genuchten (vG) and Peters–Durner–Iden (PDI-vG) functions, respectively. Left: Water retention function; right: first derivative of the water retention function. Darker colors: higher values for α. Other parameter values are n =1.2, θ_r = 0.15, and θ_s = 0.45.

absolute prediction of the HCC across the entire moisture range—covering both capillary and noncapillary conductivity—based solely on the WRC (Peters et al., 2021; Peters, Hohenbrink, et al., 2023). With this approach, the PDI model only requires the parameters of the retention curve to fully describe both hydraulic functions. For instance, when the van Genuchten function is used to represent capillary water saturation, only four free parameters are needed.

Recently, Peters et al. (2025) combined the PDI model system with the approach developed by Tian et al. (2018, 2019) to predict the effects of compaction on both hydraulic functions across the complete moisture range. They did not calibrate the model but applied the prediction scheme by Tian et al. (2018) to scale individual model parameters according to changes in bulk density. The novel model was tested with a dataset of an agricultural experimental site. To further evaluate the performance of the new approach, a more comprehensive assessment is required.

The aim of this study was to calibrate and validate the model approach of Peters et al. (2025) with a large dataset encompassing different soil textures. To achieve this aim, we used the data of Tian et al. (2018). Furthermore, two different variants of fixed and scaled parameters are compared to identify the optimal variant together with the optimal scaling parameters.

Core Ideas

- The effect of compaction on soil water retention curve is modeled across the full moisture spectrum.
- Successful model calibration was achieved with only one estimated parameter.
- Other model parameters can either be held constant or predicted from physical reasoning.
- Only reference curve and bulk density are required for predicting water retention curve of compacted soil.
- We hypothesize that the approach is independent of the model used to parametrize the pore-size distribution.

2 | THEORY

2.1 | PDI model

The PDI water retention model is basically given by the sum of a capillary and a noncapillary (adsorptive) part. The former can be any unimodal (e.g., Kosugi, 1996; van Genuchten, 1980) or multimodal (e.g., Durner, 1994; Romano et al., 2011) classic retention function, which is scaled to reach zero water content at oven dryness. The latter is a smoothed piecewise linear function of water content versus the logarithm of suction. The formulations of Peters et al. (2021) and Peters, Hohenbrink et al. (2023) allow a full prediction of the HCC from the retention function over the full moisture range. Thus, if the water retention can be predicted for any compacted state, the corresponding conductivity curve can also be predicted. The PDI model using the van Genuchten function as a basic capillary saturation function is called "PDI-vG" and is summarized in Appendix A1. We refer to Peters et al. (2024) and the citations therein for a thorough description of the model. The PDI-vG model has four unknown parameters: θ_s (-), the volumetric saturated water content; θ_r (-), the maximum water content of the noncapillary component; α (cm^{-1}), which shifts the capillary retention function along the suction axis; and n (-), the so-called pore-size distribution index.

2.2 | Prediction of PDI parameters for compacted soils

Peters et al. (2025) combined the approach of Tian et al. (2018), which was developed for the van Genuchten model, with the PDI-vG. The scaling for the parameters θ_s, α, and n is achieved by the following equations (Tian et al., 2018):

$$\frac{\theta_{s,i}}{\theta_s^*} = \frac{\rho_s - \rho_{b,i}}{\rho_s - \rho_b^*} \tag{1}$$

$$\frac{\alpha_i}{\alpha^*} = \left(\frac{\rho_{b,i}}{\rho_b^*}\right)^{-\omega} \tag{2}$$

$$\frac{n_i - 1}{n^* - 1} = \left(\frac{\rho_{b,i}}{\rho_b^*}\right)^{\varepsilon_1 + \varepsilon_2 f_s / f_c} \tag{3}$$

where the asterisk and the index i indicate the parameters of the reference and compacted soils, respectively, ρ_s (g cm^{-3}) and ρ_b (g cm^{-3}) are the solid and bulk density, ω (-), ε_1 (-), and ε_2 (-) are empirical parameters that describe the change in retention parameters α, and n with relative bulk density $\frac{\rho_{b,i}}{\rho_b^*}$, and f_s (kg kg^{-1}) and f_c (kg kg^{-1}) are the mass fractions of silt and clay. Tian et al. (2018) found that $\omega = 3.97$, $\varepsilon_1 = -0.97$, and $\varepsilon_2 = 1.28$ are good choices for describing the effect of ρ_b on the WRC for the van Genuchten (1980) model. In this contribution, we want to identify best values of these three parameters for the PDI-vG model.

Peters et al. (2025) developed a model for scaling the slope of the noncapillary retention function in the hygroscopic range. The resulting formulation for the dependence of θ_r on bulk density is:

TABLE 1 Texture, textural classes, particle density (ρ_s), bulk density (ρ_b), and source of the datasets used in this study. Note that the IDs are identical to those in Tian et al. (2018).

ID	Texture	Sand (-)	Silt (-)	Clay (-)	ρ_s (g cm^{-3})	ρ_b (g cm^{-3})	Source
1	Sand	0.9	0.06	0.04	2.71	1.50, 1.52, 1.53, 1.56	Laliberte et al. (1966)
2	Sandy loam	0.54	0.35	0.11	2.66	1.22, 1.28, 1.34, 1.44	Laliberte et al. (1966)
3	Silt loam	0.32	0.53	0.15	2.60	1.32, 1.40, 1.48	Laliberte et al. (1966)
4	Loam	0.48	0.34	0.18	2.65	0.99, 1.18, 1.32	Reicovsky et al. (1981)
6	Sandy loam	0.87	0.02	0.11	2.65	1.26, 1.41	Assouline (2006b)
7	Clay	0.30	0.10	0.60	2.65	1.06, 1.22	Or et al. (2000)
8	Sandy loam	0.70	0.21	0.09	2.47	0.68, 0.89	Moroizumi and Horino (2004)
9	Sandy loam	0.53	0.37	0.10	2.65	1.75, 1.77, 1.80, 1.82	Huang et al. (1998)
10	Sandy loam	0.72	0.18	0.10	2.65	1.32, 1.43, 1.58, 1.71, 1.84	Salager et al. (2010)
11	Loamy sand	0.88	0.05	0.07	2.66	1.50, 1.58, 1.67	Gao et al. (2012)
13	Loamy sand	0.85	0.09	0.06	2.65	1.44, 1.50, 1.55, 1.60, 1.70	Tian et al. (2018)
14	Silt loam	0.18	0.57	0.25	2.65	1.09, 1.19, 1.29, 1.38	Tian et al. (2018)
15a	Clay loam (N)	0.24	0.45	0.31	2.65	1.38, 1.56, 1.55, 1.57	Gao et al. (2016)
15b	Clay loam (R)	0.24	0.45	0.31	2.65	1.19, 1.26, 1.43, 1.52	Gao et al. (2016)
16	Silt loam	0.14	0.66	0.20	2.65	1.22, 1.32, 1.47, 1.56	Tian et al. (2018)

Note: N: no till; R: ridge-till.

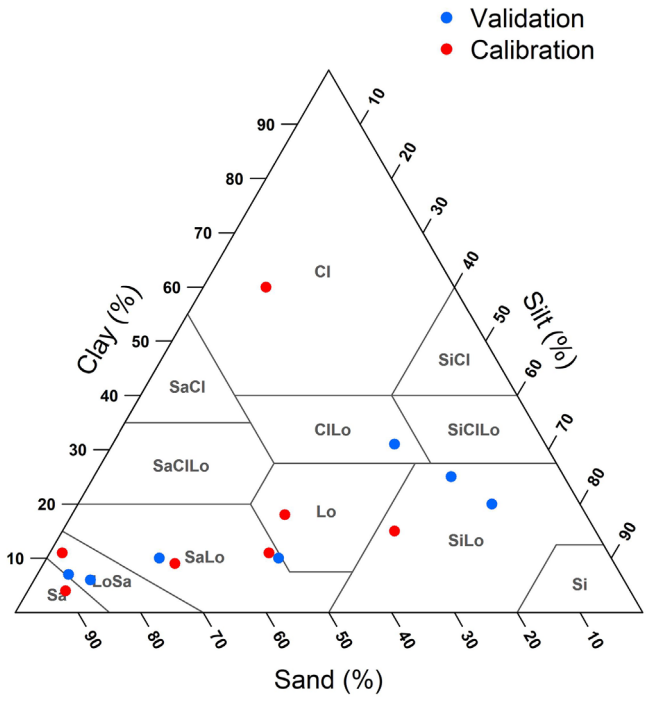

FIGURE 2 Textures of soils used for calibration and validation.

$$\frac{\theta_{r,i}}{\theta_r^*} = \frac{x_0 - x_{a,i}}{x_0 - x_a^*} \frac{\rho_{b,i}}{\rho_b^*} \tag{4}$$

where x is the common logarithm of the suction h (cm) and therefore x_0 and x_a are the common logarithms of h_0 and h_a (see Equations A2–A6), that is, $x \equiv \mathrm{pF}$, where ($\mathrm{pF} = \log_{10}(h\ [\mathrm{cm}])$). A derivation of Equation (4) is given in Appendix A2.

Summing up, Equation (1) accounts for the decrease of porosity and the associated decrease in θ_s, Equation (2) for the shift of the pore-size distribution toward finer pores, Equation (3) for the narrowing of the pore-size distribution, and Equation (4) for the increase of the volumetric water content in the hygroscopic range due to increased bulk densities, which lead to an increase in specific surface area per unit volume of soil.

In their analysis, Peters et al. (2025) found that scaling n by Equation (3) does not improve the prediction but makes it rather worse. This might contradict the expectation that the pore-size distribution should become narrower due to compaction because the volume fraction of larger pores might diminish more than the fraction of smaller pores. However, unlike the classic models, where a change in α leads only to a shift of the pore-size distribution on the pF-axis, changing α in the PDI system does also lead to a change of the widths of the pore-size distribution (Figure 1), which is most pronounced for fine textured soils. This is due to the scaling of the basic function to achieve a zero capillary water content at h_0 (Equation A2). If α decreases, the basic function (here Equation A3) is shifted toward higher pF values. This must be compensated by a steeper course of the modeled retention curve and thus a narrower pore-size distribution (Figure 1, right) to meet zero water content at the constant h_0, which is unaffected by compaction.

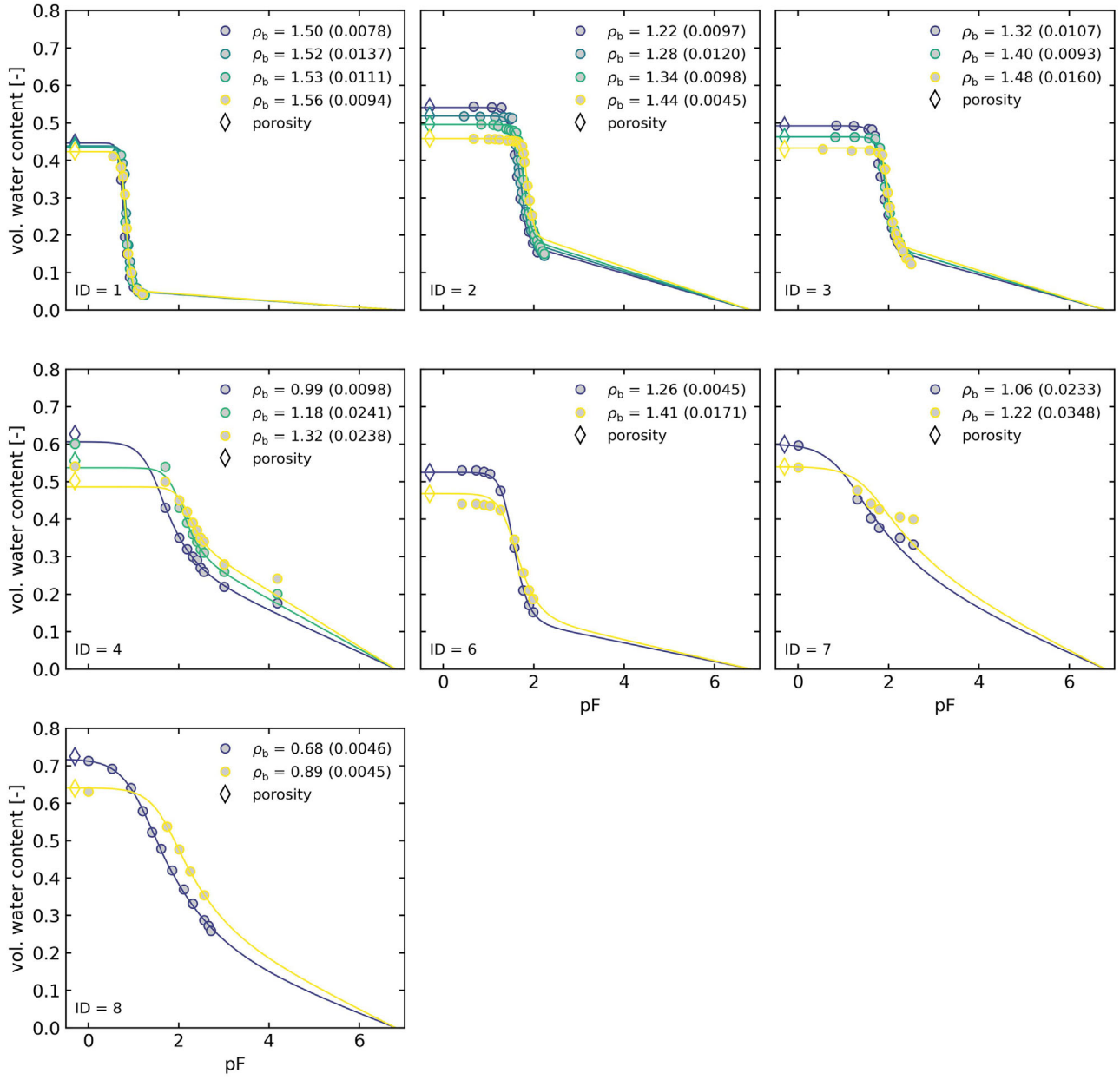

FIGURE 3 Calibration data and fitted curves of variant cal1 (α and n fitted, θ_r and θ_s predicted from ρ_b, Table 2). Numbers in brackets in legend indicate the root mean square error (RMSE) values. Data with lowest bulk densities are reference data to which all four retention parameters were adjusted.

TABLE 2 Applied schemes to the calibration data, except for the reference data.

Variant	α	n	θ_r	θ_s	n_p
cal0	Fit	Fit	Fit	Fit	4
cal1	Fit	Fit	Pred	Pred	2
cal2	Fit	Fix	Pred	Pred	1

Note: n_p, number of fitted parameters; fit, parameter is fitted; pred, parameter is predicted; fix, parameters is fixed to the reference value.

3 | MATERIALS AND METHODS

3.1 | Data source

In order to calibrate and test our approach, we used the comprehensive data collection from Tian et al. (2018). Each dataset consists of measured water retention data and corresponding bulk densities for different compaction states of a particular soil. Additionally, texture data are available for each dataset (see Table S1). In a preliminary analysis, we excluded two complete datasets (one of the calibration set and one of

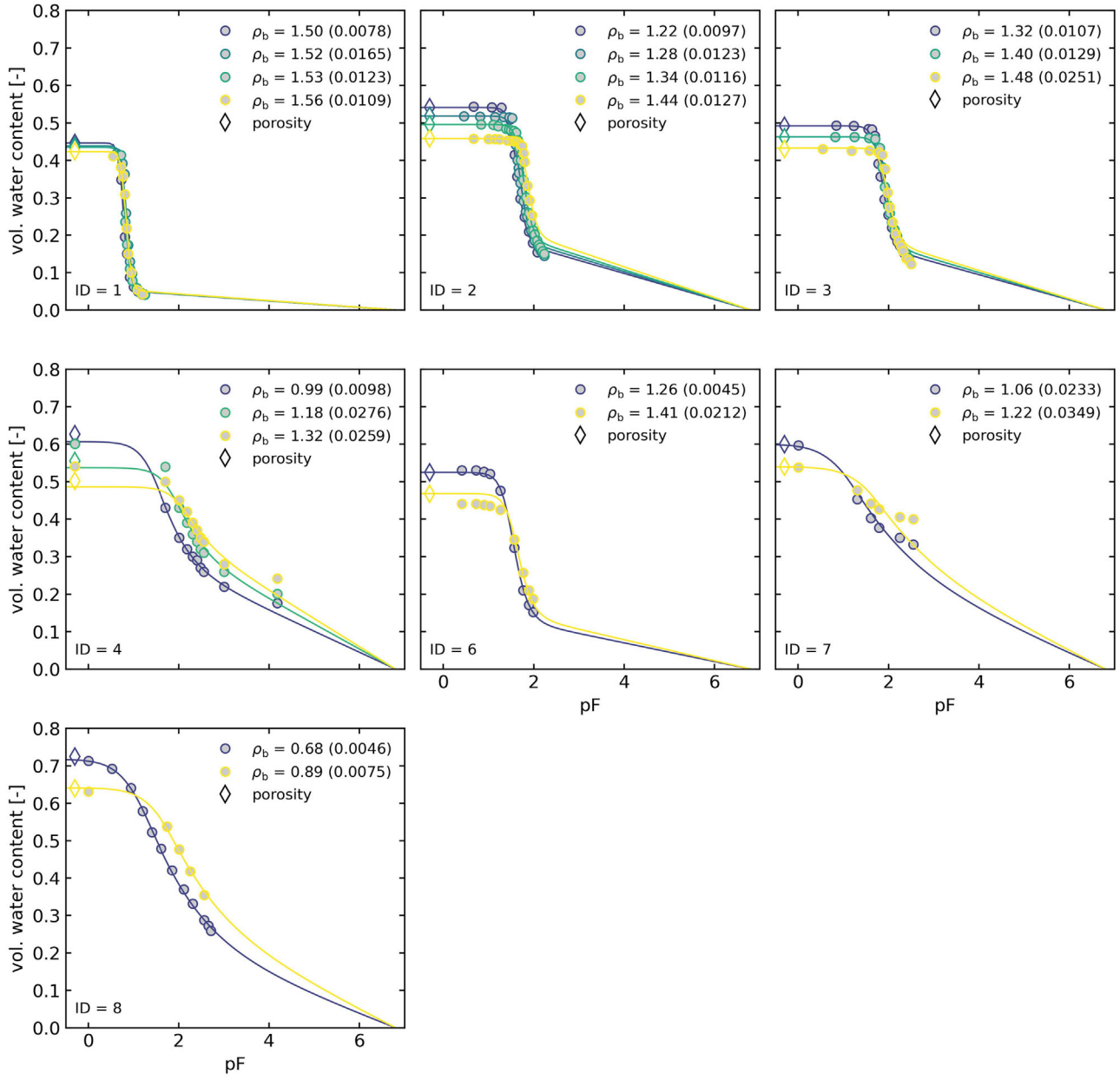

FIGURE 4 Calibration data and fitted curves of variant cal2 (α fitted, n fixed, θ_r and θ_s predicted from ρ_b, Table 2). Numbers in brackets in legend indicate the root mean square error (RMSE) values. Data with lowest bulk densities are reference data to which all four retention parameters were adjusted.

the validation set, namely, with the IDs 5 and 12) out of 17 due to inconsistencies in the data or because the data could not be accurately described by the model when all parameters were adjusted. Additionally, one subset (ID 4), specifically the data with bulk density of 1.59 g cm^{-3}, was excluded due to a poor fit when all parameters were adjusted. The results of this preliminary analysis are provided in Figures S1 and S2. For consistency, we used the same IDs as Tian et al. (2018). Table 1 summarizes the used datasets with their basic properties, like bulk and particle densities, textural information, and literature sources. In accordance with Tian et al. (2018), the data with IDs 1–8 were used for model calibration and the others for validation. The bulk and particle densities (ρ_b [g cm^{-3}] and ρ_s [g cm^{-3}]) were used to calculate the porosities (ϕ) by $\phi = 1 - \frac{\rho_b}{\rho_s}$. Figure 2 shows how the calibration and validation datasets are distributed within the texture triangle.

3.2 | Model calibration

The aim of the study was to calibrate and test the prediction scheme proposed by Peters et al. (2025) for the PDI-vG model parameters for any compaction status based on a reference.

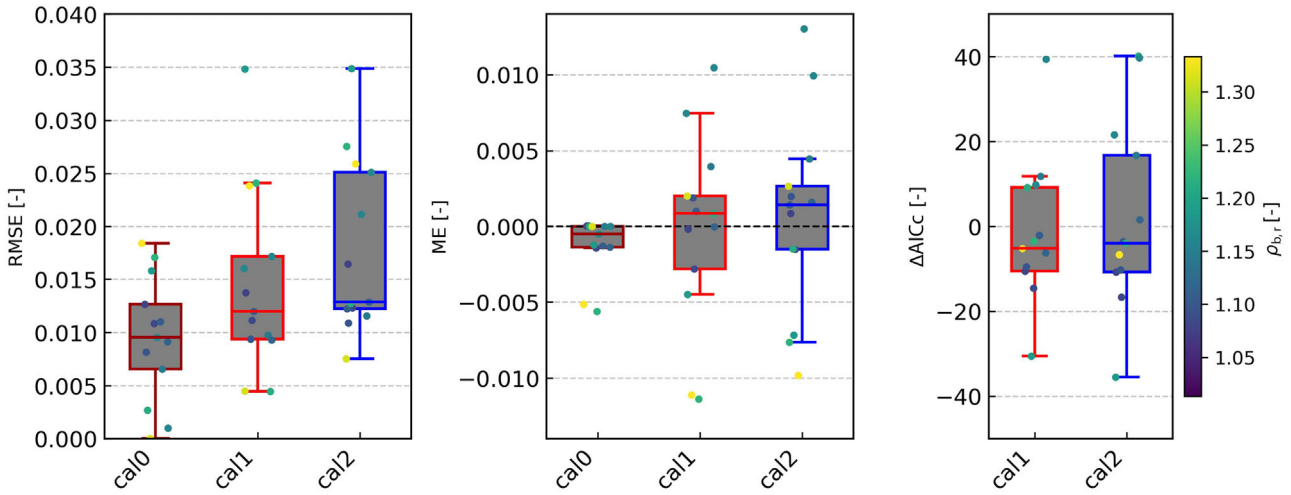

FIGURE 5 Boxplots for (root mean square error) RMSE, mean error (ME), and difference in modified Akaike information criterion (ΔAICc) for the calibration variants listed in Table 2. cal0: all parameters fitted, cal1: α and n fitted, θ_r and θ_s predicted; cal2: α fitted, n fixed, θ_r and θ_s predicted. The colors of the dots indicate the relative bulk density, $\rho_{b,r}$, given by the quotient of the bulk densities of the compacted soil and the reference.

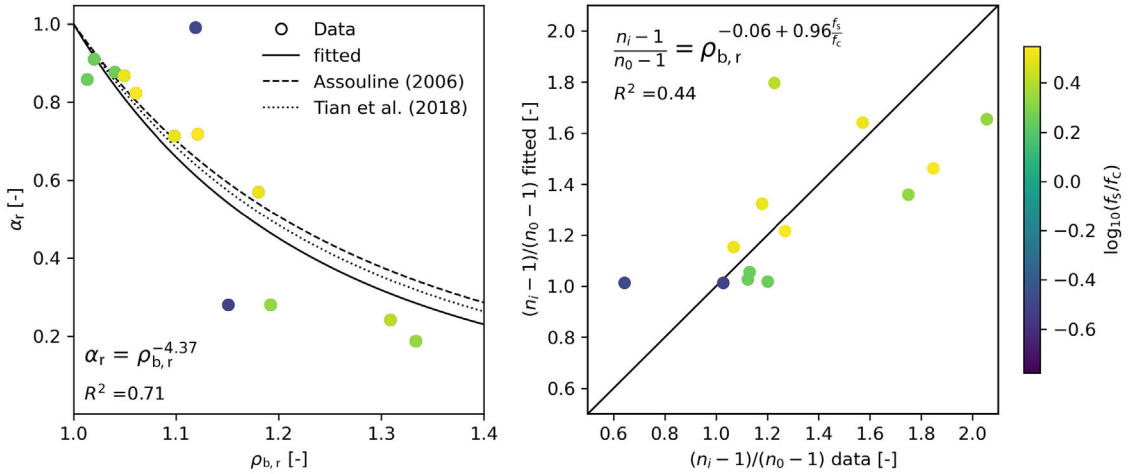

FIGURE 6 Parameter calibrations for variant cal1. Left: Relationship between fitted relative α ($\alpha_r = \frac{\alpha_i}{\alpha_0}$) and relative bulk density ($\rho_{b,r} = \frac{\rho_{b,i}}{\rho_b^*}$) for the calibration data with fitted function (Equation 2). The parameter ω was fitted and its estimated value is 4.37. Assouline (2006a) and Tian et al. (2018): Relationships for α_r versus $\rho_{b,r}$ found by these authors. Right: Relationship of fitted versus given $(n_i - 1)/(n_0 - 1)$ using Equation (3). The colors of dots indicate the log10 of the quotient of silt and clay fractions.

TABLE 3 Applied schemes to the validation data, except for the reference data.

Variant	α	n	θ_r	θ_s
val0	Fit	Fit	Fit	Fit
val1	Pred	Pred	Pred	Pred
val2	Pred	Fix	Pred	Pred
val3	Fix	Fix	Fix	Fix

Note: Pred: parameter is predicted, fix: parameter is fixed to the reference value.

The parameters θ_r and θ_s can be predicted by the Equations (4) and (1), which do not require calibration. The remaining two parameters α and n are parameters controlling the shape of the WRC and are related to bulk density by Equations (2) and (3), which require calibration. As outlined above, a shift of α does not only shift the pore-size distribution, but it also leads to a change in the width of the capillary retention function in the PDI-vG model (Figure 1).

For each dataset, the sample with the lowest bulk density was chosen as reference. First, the PDI-vG model was fitted to the reference data, adjusting all four parameters, namely, α, n, θ_r and θ_s. Then, we tested two different calibration schemes for the data with higher bulk density: (i) Predict θ_r and θ_s by Equations (4) and (1) and fit α and n (cal1), and (ii) predict θ_r and θ_s, fix n at the reference value and fit only α (cal2).

TABLE 4 Statistical measures for the validation data. The measures for the references are given in bold. The means and medians are calculated excluding the reference values. Numbers in brackets in first column indicate contents of sand, silt, and clay.

		Val1			Val2		
ID (texture)	**ρ_b (g cm^{-3})**	**RMSE**	**ME**	**R^2**	**RMSE**	**ME**	**R^2**
9 (0.53, 0.37, 0.10)	**1.75**	**0.0035**	**0.00003**	**0.998**	**0.0035**	**0.00003**	**0.998**
	1.77	0.0051	−0.00240	0.996	0.0053	−0.00209	0.996
	1.80	0.0079	−0.00608	0.995	0.0081	−0.00548	0.995
	1.80	0.0076	−0.00698	0.997	0.0075	−0.00630	0.997
10 (0.72, 0.18, 0.10)	**1.32**	**0.0112**	**−0.00242**	**0.993**	**0.0112**	**−0.00242**	**0.993**
	1.43	0.0126	−0.00730	0.992	0.0095	−0.00225	0.993
	1.58	0.0338	−0.03066	0.966	0.0251	−0.02227	0.978
	1.71	0.0319	−0.02580	0.941	0.0264	−0.02060	0.955
	1.84	0.0345	−0.02914	0.959	0.0292	−0.02407	0.972
11 (0.88, 0.05, 0.07)	**1.50**	**0.0170**	**−0.00110**	**0.966**	**0.0170**	**−0.00110**	**0.966**
	1.58	0.0251	−0.02084	0.979	0.0241	−0.01995	0.980
	1.67	0.0324	−0.02129	0.920	0.0309	−0.01992	0.924
13 (0.85, 0.09, 0.06)	**1.44**	**0.0079**	**0.00047**	**0.996**	**0.0079**	**0.00047**	**0.996**
	1.50	0.0116	0.00433	0.993	0.0125	0.00494	0.993
	1.55	0.0222	0.00886	0.970	0.0229	0.00968	0.969
	1.60	0.0157	−0.00832	0.997	0.0167	−0.00751	0.996
	1.70	0.0293	0.01161	0.928	0.0282	0.01196	0.935
14 (0.18, 0.57, 0.25)	**1.09**	**0.0278**	**−0.00543**	**0.959**	**0.0278**	**−0.00543**	**0.959**
	1.19	0.0336	−0.02363	0.960	0.0285	−0.01392	0.956
	1.29	0.0390	−0.03439	0.972	0.0296	−0.02089	0.962
	1.38	0.0287	−0.02140	0.978	0.0247	−0.00838	0.954
15a (0.24, 0.45, 0.31)	**1.38**	**0.0180**	**−0.00506**	**0.992**	**0.0180**	**−0.00506**	**0.992**
	1.56	0.0385	−0.03133	0.999	0.0353	−0.02917	0.999
	1.55	0.0451	−0.03708	0.989	0.0420	−0.03488	0.989
	1.57	0.0432	−0.02801	0.970	0.0398	−0.02579	0.970
15b (0.24, 0.45, 0.31)	**1.19**	**0.0142**	**−0.00436**	**0.996**	**0.0142**	**−0.00436**	**0.996**
	1.26	0.0370	−0.02734	0.998	0.0341	−0.02439	0.999
	1.43	0.0324	−0.02609	0.984	0.0268	−0.02079	0.987
	1.52	0.0419	−0.04016	0.995	0.0367	−0.03553	0.999
16 (0.14, 0.66, 0.20)	**1.22**	**0.0192**	**0.00001**	**0.980**	**0.0192**	**0.00001**	**0.980**
	1.32	0.0212	−0.00969	0.983	0.0154	−0.00046	0.986
	1.47	0.0224	−0.01843	0.986	0.0118	−0.00587	0.989
	1.56	0.0199	−0.01611	0.985	0.0139	−0.00550	0.990
Mean		0.0269	−0.01791	0.977	0.0234	−0.01318	0.979
Median		0.0293	−0.02129	0.984	0.0251	−0.01392	0.987

Abbreviations: ME, mean error; RMSE, root mean square error.

For comparison, we also fitted all 4 parameters for these data (cal0). The schemes are summarized in Table 2. The datasets with IDs 1–8 (Table 1) were used for calibration.

To ensure that the noncapillary water content, θ_{nc}, consistently reflects the water content at pF 5.8, we enforced a constraint during parameter optimization, requiring that $\theta_{nc} \geq 0.95\theta$ at pF 5.8 (Peters et al., 2025). Furthermore, the maximum allowed noncapillary water content (θ_r) was set to $0.5\theta_s$ for the reference and to $0.9\theta_s$ for the compacted soils during parameter optimization. The former ensures that adsorptive water content was allowed to increase sufficiently for higher bulk densities, and the latter ensures that scaling of the parameters does not lead to unphysically high adsorptive water contents.

Fitting was done with SHYPFIT2.0 (Peters & Durner, 2015), which applies the shuffled complex evolution

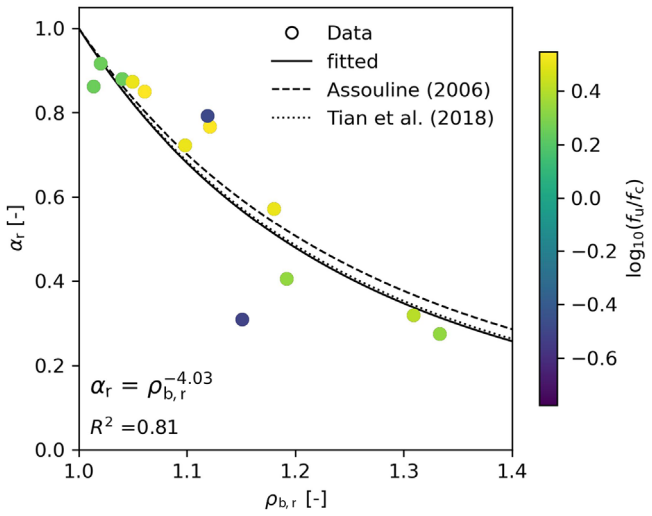

FIGURE 7 Relationship between fitted relative α ($\alpha_r = \frac{\alpha_i}{\alpha_0}$) and relative bulk density ($\rho_{b,r} = \frac{\rho_{b,i}}{\rho_b^*}$) for the calibration data with fitted function (Equation 2) for variant cal2 with fixed n. The parameter ω was fitted and its estimated value is 4.03. The colors of dots indicate the log10 of the quotient of silt and clay fractions. Assouline (2006a) and Tian et al. (2018): Relationships for α_r versus $\rho_{b,r}$ found by these authors.

algorithm of Duan et al. (1992) for minimizing the objective function. The fitting performance was evaluated by calculating the root mean square error (RMSE), the mean error (ME), the coefficient of determination (R^2), and the modified Akaike information criterion (AICc) (Hurvich & Tsai, 1989). The latter is given by:

$$\mathrm{AICc} = n_d \ln\left(\frac{\mathrm{SSQ}}{n_d}\right) + 2n_p + \frac{2n_p\left(n_p+1\right)}{n_d - n_p - 1} \quad (5)$$

where SSQ is the sum of squared residuals (minimized function), n_p is the number of adjusted parameters, and n_d is the number of data points. Since the volumetric water content is dimensionless, RMSE, ME, and AICc are also dimensionless. The RMSE gives information about the dispersion of observed values around the model, the ME about the bias, and the AICc can help to select the superior scheme, rewarding the goodness of fit, and penalizing for the number of adjusted parameters. The lower the AICc, the better the model. Since the value of the AICc itself depends on the number of data among others, we do not analyze the AICc but the difference in AICc of the full fit (variant 0: AICc_0) and the AICc of the variant of interest (AICc_i): $\Delta\ \mathrm{AICc}_i = \mathrm{AICc}_0 - \mathrm{AICc}_i$.

Finally, the parameters ω, ε_1, and ε_2 were estimated by adjusting Equations (2) and (3) to the estimated values for α and n by nonlinear regression.

3.3 | Model validation

To validate the prediction scheme, we used the data with IDs 9–17 (Table 1). Again, the PDI-vG model was fitted to the reference data (lowest bulk density) by adjusting all four parameters. The validation is similarly constructed as the calibration with the variants given in Table 2. The parameters α, n, θ_r and θ_s for the remaining datasets were predicted using Equations (1)–(4) or fixed to the reference values. Hence, the parameters that were fitted in the calibration were now predicted by Equations (1)–(4). An overview is given in Table 3. Variant val1 resembles the variant used in Tian et al. (2018) for the van Genuchten model. In addition to the variants of the calibration scheme, we added variant val3, in which the reference parameters are used to describe the behavior of the compacted soil, that is, the effect of bulk density on the retention curve is neglected. Again, the prediction performance was evaluated by calculating the RMSE, ME, and R^2.

4 | RESULTS AND DISCUSSION

4.1 | Calibration

4.1.1 | Fitting retention curve parameters

Figures 3 and 4 show all used calibration data and the fitted model applying variant cal1 (fitting a and n, predicting θ_s and θ_r from ρ_b) and variant cal2 (fitting a, fixing n, predicting θ_s, and θ_r from ρ_b), respectively. Except for the soil with ID 7, all data are well described by both variants. The difference between the two seems to be minimal. As expected, fitting a and n further reduces the RMSE as compared to the variant where only a is fitted. This is also reflected in Figure 5 and TableA1, which summarize the statistical measures. All three measures indicate a very good performance of both variants and are only slightly worse than those of the full fit as already indicated in Figure 5. This is remarkable since only two or one of the four parameters were fitted, whereas the others were predicted or kept at their reference values. The median RMSE for variants cal1 and cal2 was 0.012 and 0.013, respectively. Interestingly, the ME is not further reduced by including n in the calibration. The median ME was close to zero for these two variants with 0.0009 and 0.0014, respectively. The AICc was alike for both variants with a slightly better performance of variant cal2 (fixed n), which had a lower AICc for 8 out of 13 realizations (see also Table A2). The slight superiority of variant cal2 with respect to the AICc can be attributed to the fact that, even with a fixed n, the pore-size distribution narrows for fine-textured soils, when a becomes smaller (Figure 1). Summarizing,

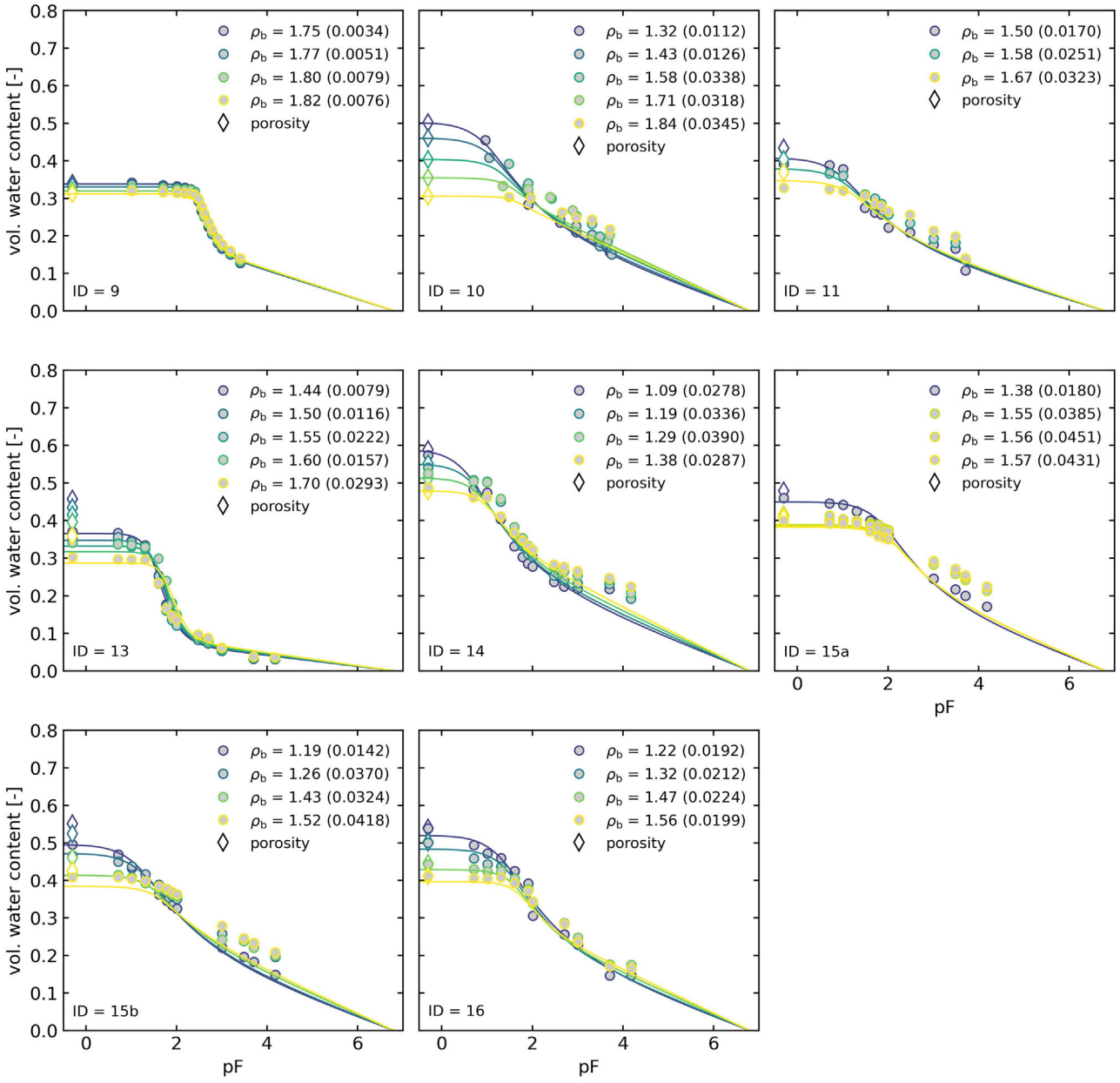

FIGURE 8 Validation data and predicted curves of variant val1, that is, all parameters are predicted using Equations (1)–(4) with the scaling parameters for α and n derived in Section 4.1.2. Numbers in brackets in legend indicate the root mean square error (RMSE) values. Data with lowest bulk densities are reference data to which all four retention parameters were adjusted.

variants cal1 and cal2 show almost similar performance, with variant cal2 performing slightly better according to the AICc when calibrating the model. The estimated, fixed, and predicted parameters for all calibration datasets for variant cal2 are summarized in Table A3. Note that the findings of Peters et al. (2025)—who observed that keeping θ_s at its reference value was superior for their dataset—cannot be generalized. This becomes evident when examining the data (Figures 3 and 4), which show that both porosity and saturated water content decrease with increasing bulk density.

4.1.2 | Fitting scaling parameters

In this section, the prediction schemes for the hydraulic parameters α and n are derived. Figure 6, left shows the relative value of α, $\alpha_r = \frac{\alpha_i}{\alpha_0}$, versus the relative bulk density, $\rho_{b,r} = \frac{\rho_{b,i}}{\rho_{b,0}}$, with the fitted Equation (2) for variant cal1. The parameter ω was estimated to be 4.37 with an R^2 of 0.71. Tian et al. (2018) derived the value 3.97 for the van Genuchten (1980) model and Assouline (2006a) derived 3.72 for his retention model. Hence, the parameter α, which scales the capillary retention with respect to suction, might be regarded as model

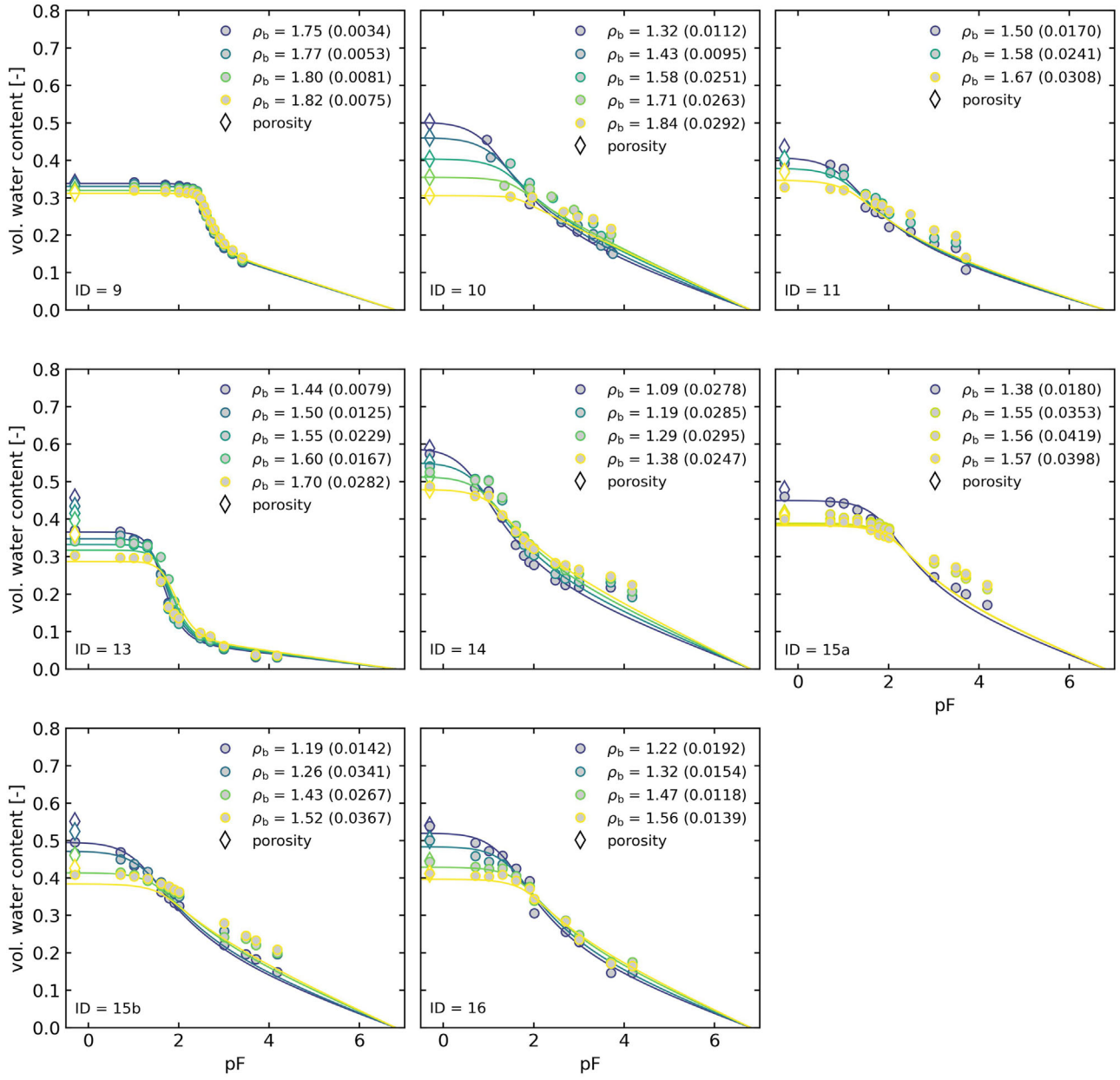

FIGURE 9 Validation data and predicted curves of variant val2, that is, parameters θ_r, θ_s and α are predicted using Equations (1), (2), and (4) with the scaling parameters for α derived in Section 4.1.2, and n was fixed to the reference value. Numbers in brackets in legend indicate the root mean square error (RMSE) values. Data with lowest bulk densities are reference data to which all four retention parameters were adjusted.

independent, and we may generally set ω to 4.0. The relative values for n, that is, $(n_i - 1)/(n_0 - 1)$, could only weakly be described by Equation (3) with an R^2 of 0.44 (Figure 6, right). The parameters in the exponent of Equation (3), ε_1 and ε_2 have now the values −0.06 and 0.96.

The relationship of α_r and $\rho_{b,r}$ for variant cal2 is shown in Figure 7. Now, the value of ω is 4.03 and thus even closer to the values derived by Tian et al. (2018) and Assouline (2006a), respectively. Additionally, the R^2 is now higher in the case of variant cal1 with 0.81.

4.2 | Validation

In this section, the calibrated prediction schemes for variants cal1 and cal2 are tested with the validation datasets. Figure 8 shows the validation data with the predicted WRCs for variant val1, that is, with all four parameters predicted using Equations (1)–(4) with the newly derived scaling parameters for Equations (2) and (3). Overall, the prediction is fairly sound; however, for soils 10, 11, 14, 15a, and 15b, there is a clear underprediction in the dry range (above pF 3 [≙ 1000 cm]).

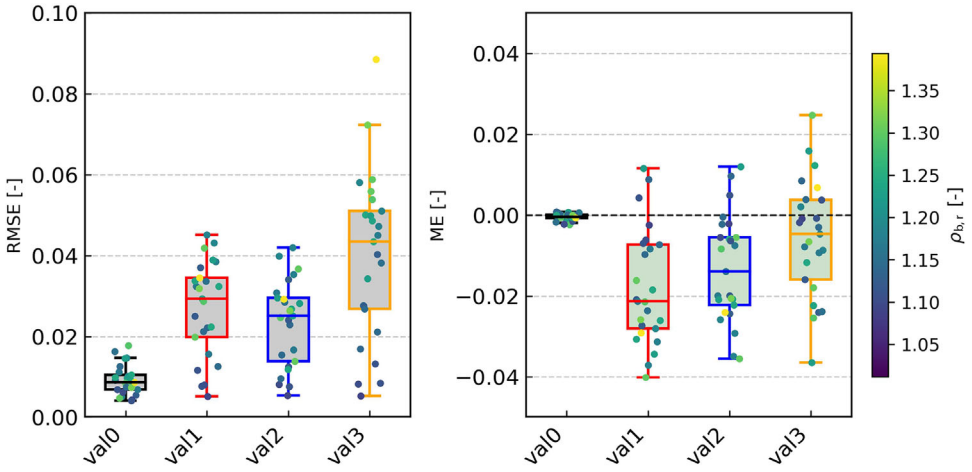

FIGURE 10 Boxplots for root mean square error (RMSE) and mean error (ME) for all validation variants (Table 3). val0: all parameters fitted, val1: all parameters predicted; val2: α, θ_r, and θ_s predicted, and n fixed; val3: all parameters are fixed to the reference values. The colors of the dots indicate the relative bulk density, $\rho_{b,r}$, given by the quotient of the bulk densities of the compacted soil and the reference.

Note that for soils 11, 14, and 15a, this underprediction occurs even for the fit of the reference curve (lowest bulk density).

Remarkably, prediction of the WRCs using variant val2 (fixed n) leads to slightly better matches between model and data (Figure 9), which were not found alike in the calibration (Figures 3–5). The better performance of variant val2 can also be seen in Figure 10. The statistical measures are summarized in Table 4. The median RMSE and ME were 0.029 and −0.021 for variant val1 and 0.025 and −0.014 for variant val2. The median R^2 are 0.984 and 0.987, respectively. Tian et al. (2018) reported a mean RMSE for their variant of 0.025, which is slightly higher than the mean RMSE of 0.023 in our variant val2. Interestingly, the mean R^2 for val2 was 0.987, whereas it was 0.94 in Tian et al. (2018). The better performance with respect to the R^2 indicates a lower model error of the PDI model as compared to the van Genuchten (1980) model. The predicted and fixed parameters for all calibration datasets for variant val2 are summarized in Table A4.

Note that the "shift-parameter" α is independent of the underlying model for capillary saturation (S_c), whereas the parameter (or parameters), that account for the widths of S_c, in our case n, might differ for the different S_c-models. As expected, the variant val3 (all parameters fixed) did not perform well. The predicted WRCs for this variant, val3, are shown in Figure S3.

Except for the direct fit (variant val0), all variants show a bias, as indicated by the ME (Figure 10; Table 4). This bias was particularly pronounced in the dry moisture range (Figures 8 and 9). To address this, we divided the data into two groups: (i) data in the moist range with $h < 1000$ cm (pF < 3) and (ii) data in the dry range with $h \geq 1000$ cm (pF ≥ 3). Comparing the prediction schemes across these subsets confirms that the bias for $h < 1000$ cm is indeed very small (Figure A2), especially for variant val2, whereas it is relatively large in the dry range. The bias in the dry range can either be attributed to a model error or to erroneous measurements in that range. The former is supported by the limited flexibility of the unimodal constrained capillary saturation model used in this study. The latter is supported by the measurement method: for soils 14, 15a, and 15b, which exhibit a large bias, the data in the dry range were obtained using a pressure chamber apparatus. Bittelli and Flury (2009) and Solone et al. (2012) found that measurements in the dry range with pressure plates are often affected by contact issues, leading to overestimated water content, particularly in fine-textured soils. To address this problem, data are needed that are obtained using methods capable of providing high-resolution measurements with reduced susceptibility to errors, for example, the simplified evaporation method (Peters & Durner, 2008; Peters et al., 2015; Schindler, 1980) in combination with the dew point method (Campbell et al., 2007) can be used to measure the SHPs of compacted and uncompacted soils.

5 | SUMMARY AND CONCLUSIONS

The recently developed model for predicting compaction effects on SHPs across the full moisture range by Peters et al. (2025) was calibrated and tested using a dataset that encompasses a wide variety of soil texture. The model is a combination of the PDI model system for parameterizing SHPs (Peters et al., 2024) and the approach of Tian et al. (2018) to parameterize the effect of compaction on the WRC. The soil water retention model is described by four parameters, namely, θ_s, θ_r, α and n. The first two can be scaled by physical reasoning using Equations (1) and (4) and do not

require calibration. The parameters, α, which shifts the capillary saturation function on the suction axis, and n, which is a shape parameter that accounts for the width of the pore-size distribution, had to be calibrated. Two different variants, which vary in the number of degrees of freedom have been tested. The variant that only scales α and treats n as a constant, obtained at the reference bulk density turned out to be superior. Fixing n to the reference value aligns with the findings of Peters et al. (2025). However, their finding that θ_s also needed to be fixed to the reference value, likely due to entrapped air in the reference samples, could not be confirmed.

The commonly used capillary retention functions—such as the unimodal models by van Genuchten (1980), Kosugi (1996), or their multimodal counterparts by Durner (1994) and Romano et al. (2011)—all include parameters that shift the location of the pore-size distribution. As a consequence, our calibration of the change in α as function of bulk density has the potential to be model-independent. Therefore, if soils exhibit more complex pore-size distributions and must be described by other retention models, scaling of α, θ_s, θ_r, as described above, might be done without new calibration using Equations (1), (2) and (4). The scaling parameter ω in Equation (2) can be simply set to 4.0. An additional advantage of fixing the parameter n over scaling it by Equation (3) is that no information on texture is required. Hence, the reference curve and the bulk densities provide sufficient information for modeling the effect of compaction on the WRC. By combining this approach with the hydraulic conductivity prediction schemes proposed by Peters et al. (2021) and Peters, Hohenbrink et al. (2023), a full prediction of the complete SHP functions across the entire moisture range is achievable. These predictions require solely the reference retention curve and bulk density data.

Most data in our study were obtained from pressure or suction plate apparatuses and similar devices with limited resolution and, in case of the pressure chambers, questioned accuracy. Measurements using the simplified evaporation method (Peters & Durner, 2008; Peters et al., 2015; Schindler, 1980), which provides high-resolution data, combined with the dew point method (Campbell et al., 2007; Kirste et al., 2019) could help determine whether more complex models are needed and could increase the accuracy of the identified scaling relations involving empirical parameters like ω. For example, the combination of the PDI system with the capillary saturation function by Fredlund and Xing (1994), as proposed by Peters, Iden et al. (2023), or even the use of bi- or multimodal capillary saturation functions, could be further investigated.

AUTHOR CONTRIBUTIONS

Andre Peters: Conceptualization; data curation; formal analysis; investigation; methodology; software; validation; visualization; writing—original draft; writing—review and editing. **Zhengchao Tian**: Data curation; writing—review and editing. **Joshua L. Heitman**: Data curation; writing—review and editing. **Sascha C. Iden**: Formal analysis; writing—review and editing. **Lennart Rolfes**: Data curation; writing—review and editing. **Kai Germer**: Writing—review and editing. **Marco Lorenz**: Funding acquisition; project administration; resources; writing—review and editing.

ACKNOWLEDGMENTS

This research was conducted within the SOILAssist project and has been funded by the German Federal Ministry of Education and Research (BMBF) as part of the BonaRes initiative (grant no.: 031B1065A).

Open access funding enabled and organized by Projekt DEAL.

CONFLICT OF INTEREST STATEMENT

The authors declare no conflicts of interest.

ORCID

Andre Peters https://orcid.org/0000-0002-8893-8102
Zhengchao Tian https://orcid.org/0000-0002-2088-6051
Joshua L. Heitman https://orcid.org/0000-0002-8708-0693
Sascha C. Iden https://orcid.org/0000-0001-8292-9048
Lennart Rolfes https://orcid.org/0009-0002-1646-7361
Kai Germer https://orcid.org/0000-0002-8192-6387
Marco Lorenz https://orcid.org/0009-0004-9825-4777

REFERENCES

Allbrook, R. F. (1986). Effect of skid trail compaction on a volcanic soil in central Oregon. *Soil Science Society of America Journal*, *50*(5), 1344–1346. https://doi.org/10.2136/sssaj1986.03615995005000050052x

Assouline, S. (2006a). Modeling the relationship between soil bulk density and the water retention curve. *Vadose Zone Journal*, *5*(2), 554–563. https://doi.org/10.2136/vzj270004005.0083

Assouline, S. (2006b). Modeling the relationship between soil bulk density and the hydraulic conductivity function. *Vadose Zone Journal*, *5*(2), 697–705. https://doi.org/10.2136/vzj270004005.0084

Bittelli, M., & Flury, M. (2009). Errors in water retention curves determined with pressure plates. *Soil Science Society of America Journal*, *73*, 1453–1460. https://doi.org/10.2136/sssaj2008.0082

Bruand, A., & Cousin, I. (1995). Variation of textural porosity of a clay-loam soil during compaction. *European Journal of Soil Science*, *46*(3), 377–385. https://doi.org/10.1111/j.1365-2389.1995.tb01334.x

Campbell, G. S., Smith, D. M., & Teare, B. L. (2007). Application of a dewpoint method to obtain the soil water characteristic. In T. Schanz (Ed.), *Experimental unsaturated soil mechanics* (pp. 71–77). Springer.

Duan, Q., Sorooshian, S., & Gupta, V. (1992). Effective and efficient global optimization for conceptual rainfall-runoff models. *Water Resources Research*, *28*(4), 1015–1031. https://doi.org/10.1029/91WR02985

Durner, W. (1994). Hydraulic conductivity estimation for soils with heterogeneous pore structure. *Water Resources Research*, *30*(2), 211–223. https://doi.org/10.1029/93WR02676

Duttmann, R., Augustin, K., Brunotte, J., & Kuhwald, M. (2022). Modeling of field traffic intensity and soil compaction risks in agricultural landscapes. In *Advances in understanding soil degradation* (pp. 313–331). Springer.

Fredlund, D. G., & Xing, A. (1994). Equations for the soil-water characteristic curve. *Canadian Geotechnical Journal*, *31*(4), 521–532. https://doi.org/10.1139/t94-061

Gao, W., Whalley, W. R., Tian, Z., Liu, J., & Ren, T. (2016). A simple model to predict soil penetrometer resistance as a function of density, dryingand depth in the field. *Soil & Tillage Research*, *155*, 190–198. https://doi.org/10.1016/j.still.2015.08.004

Gao, W., Watts, C. W., Ren, T., & Whalley, W. R. (2012). The effects of compaction and soil drying on penetrometer resistance. *Soil & Tillage Research*, *125*, 14–22. https://doi.org/10.1016/j.still.2012.07.006

Gupta, S. C., Sharma, P. P., & DeFranchi, S. A. (1989). Compaction effects on soil structure. *Advances in Agronomy*, *42*, 311–338. https://doi.org/10.1016/S0065-2113(08)60528-3

Hill, J. N. S., & Sumner, M. E. (1967). Effect of bulk density on moisture characteristics of soils. *Soil Science*, *103*(4), 234–238. https://doi.org/10.1097/00010694-196704000-00002

Horn, R. (2003). Stress-strain effect in structured unsaturated soils on coupled mechanical and hydraulic processes. *Geoderma*, *116*, 77–88. https://doi.org/10.1016/S0016-7061(03)00095-8

Huang, S., Barbour, S. L., & Fredlund, D. G. (1998). Development and verification of a coefficient of permeability function for a deformable-unsaturated soil. *Canadian Geotechnical Journal*, *35*(3), 411–425. https://doi.org/10.1139/t98-010

Hurvich, C. M., & Tsai, C. L. (1989). Regression and time series model selection in small samples. *Biometrika*, *76*(2), 297–307. https://doi.org/10.1093/biomet/76.2.297

Iden, S. C., & Durner, W. (2014). Comment on "Simple consistent models for water retention and hydraulic conductivity in the complete moisture range" by A. Peters. *Water Resources Research*, *50*(9), 7530–7534. https://doi.org/10.1002/2014WR015937

Kirste, B., Iden, S. C., & Durner, W. (2019). Determination of the soil water retention curve around the wilting point: Optimized protocol for the dewpoint method. *Soil Science Society of America Journal*, *83*(2), 288–299. https://doi.org/10.2136/sssaj2018.08.0286

Kosugi, K. I. (1996). Lognormal distribution model for unsaturated soil hydraulic properties. *Water Resources Research*, *32*(9), 2697–2703. https://doi.org/10.1029/96WR01776

Laliberte, G. E., Corey, A. T., & Brooks, R. H. (1966). *Properties of unsaturated porous media* (Hydrology Paper 17). Colorado State University.

McPhee, J. E., Antille, D. L., Tullberg, J. N., Doyle, R. B., & Boersma, M. (2020). Managing soil compaction–A choice of low-mass autonomous vehicles or controlled traffic? *Biosystems Engineering*, *195*, 227–241. https://doi.org/10.1016/j.biosystemseng.2020.05.006

Moroizumi, T., & Horino, H. (2004). Tillage effects on subsurface drainage. *Soil Science Society of America Journal*, *68*(4), 1138–1144. https://doi.org/10.2136/sssaj2004.1138

Mualem, Y. (1976). A new model for predicting the hydraulic conductivity of unsaturated porous media. *Water Resources Research*, *12*(3), 513–522. https://doi.org/10.1029/WR012i003p00513

Mualem, Y., & Assouline, S. (1989). Modeling soil seal as a nonuniform layer. *Water Resources Research*, *25*(10), 2101–2108. https://doi.org/10.1029/WR025i010p02101

Ngo-Cong, D., Antille, D. L., van Genuchten, M. Th., Nguyen, H. Q., Tekeste, M. Z., Baillie, C. P., & Godwin, R. J. (2021). A modeling framework to quantify the effects of compaction on soil water retention and infiltration. *Soil Science Society of America Journal*, *85*(6), 1931–1945. https://doi.org/10.1002/saj2.20328

O'Sullivan, M. F., & Simota, C. (1995). Modelling the environmental impacts of soil compaction: A review. *Soil and Tillage Research*, *35*(1–2), 69–84. https://doi.org/10.1016/0167-1987(95)00478-B

Or, D., Leij, F. J., Snyder, V., & Ghezzehei, T. A. (2000). Stochastic model for posttillage soil pore space evolution. *Water Resources Research*, *36*(7), 1641–1652. https://doi.org/10.1029/2000WR900092

Peters, A. (2013). Simple consistent models for water retention and hydraulic conductivity in the complete moisture range. *Water Resources Research*, *49*(10), 6765–6780. https://doi.org/10.1002/wrcr.20548

Peters, A. (2014). Reply to comment by S. Iden and W. Durner on "Simple consistent models for water retention and hydraulic conductivity in the complete moisture range". *Water Resources Research*, *50*(9), 7535–7539. https://doi.org/10.1002/2014WR016107

Peters, A., & Durner, W. (2008). Simplified evaporation method for determining soil hydraulic properties. *Journal of Hydrology*, *356*(1–2), 147–162. https://doi.org/10.1016/j.jhydrol.2008.04.016

Peters, A., & Durner, W. (2015). *SHYPFIT 2.0 user's manual*. Institut für Ökologie, Technische Universität Berlin.

Peters, A., Durner, W., & Iden, S. C. (2024). The PDI model system for parameterizing soil hydraulic properties. *Vadose Zone Journal*, *23*, e20338. https://doi.org/10.1002/vzj270004.20338

Peters, A., Germer, K., Naseri, M., Rolfes, L., & Lorenz, M. (2025). Modeling compaction effects on hydraulic properties of soils using limited information. *Soil and Tillage Research*, *246*, 106349. https://doi.org/10.1016/j.still.2024.106349

Peters, A., Hohenbrink, T. L., Iden, S. C., & Durner, W. (2021). A simple model to predict hydraulic conductivity in medium to dry soil from the water retention curve. *Water Resources Research*, *57*(5), e2020WR029211, https://doi.org/10.1029/2020WR029211

Peters, A., Hohenbrink, T. L., Iden, S. C., van Genuchten, M. Th., & Durner, W. (2023). Prediction of the absolute hydraulic conductivity function from soil water retention data. *Hydrology and Earth System Sciences*, *27*(7), 1565–1582. https://doi.org/10.5194/hess-27-1565-2023

Peters, A., Iden, S. C., & Durner, W. (2015). Revisiting the simplified evaporation method: Identification of hydraulic functions considering vapor, film and corner flow. *Journal of Hydrology*, *527*, 531–542.

Peters, A., Iden, S. C., & Durner, W. (2023). Prediction of absolute unsaturated hydraulic conductivity–comparison of four different capillary bundle models. *Hydrology and Earth System Sciences*, *27*(24), 4579–4593. https://doi.org/10.5194/hess-27-4579-2023

Reicovsky, D. C., Voorhees, W. B., & Radke, J. K. (1981). Unsaturated water flow through a simulated wheel track. *Soil Science Society of America Journal*, *45*, 3–8. https://doi.org/10.2136/sssaj1981.03615995004500010001x

Romano, N., Nasta, P., Severino, G., & Hopmans, J. W. (2011). Using bimodal lognormal functions to describe soil hydraulic properties. *Soil Science Society of America Journal*, *75*(2), 468–480. https://doi.org/10.2136/sssaj2010.0084

Salager, S., El Youssoufi, M. S., & Saix, C. (2010). Definition and experimental determination of a soil-water retention surface. *Cana-*

dianGeotechnical Journal, *47*(6), 609–622. https://doi.org/10.1139/T09-123

Schaap, M. G., & Leij, F. J. (2000). Improved prediction of unsaturated hydraulic conductivity with the Mualem-van Genuchten model. *Soil Science Society of America Journal*, *64*, 843–851. https://doi.org/10.2136/sssaj2000.643843x

Schindler, U. (1980). Ein Schnellverfahren zur Messung der Wasserleitfähigkeit im teilgesättigten Boden an Stechzylinderproben. *Archiv für Acker- und Pflanzenbau und Bodenkunde*, *24*, 1–7.

Soane, B. D., & Van Ouwerkerk, C. (1994). Soil compaction problems in world agriculture. In *Developments in agricultural engineering* (Vol. 11, pp. 1–21). Elsevier. https://doi.org/10.1016/B978-0-444-88286-8.50009-X

Solone, R., Bittelli, M., Tomei, F., & Morari, F. (2012). Errors in water retention curves determined with pressure plates: Effects on the soil water balance. *Journal of Hydrology*, *470–471*, 65–74. https://doi.org/10.1016/j.jhydrol.2012.08.017

Tian, Z., Gao, W., Kool, D., Ren, T., Horton, R., & Heitman, J. L. (2018). Approaches for estimating soil water retention curves at various bulk densities with the extended van Genuchten model. *Water Resources Research*, *54*(8), 5584–5601. https://doi.org/10.1029/2018WR022871

Tian, Z., Kool, D., Ren, T., Horton, R., & Heitman, J. L. (2019). Approaches for estimating unsaturated soil hydraulic conductivities at various bulk densities with the extended Mualem-van Genuchten model. *Journal of Hydrology*, *572*, 719–731. https://doi.org/10.1016/j.jhydrol.2019.03.027

Tullberg, J. (2010). Tillage, traffic and sustainability—A challenge for ISTRO. *Soil and Tillage Research*, *111*(1), 26–32. https://doi.org/10.1016/j.still.2010.08.008

Usowicz, B., & Lipiec, J. (2021). Spatial variability of saturated hydraulic conductivity and its links with other soil properties at the regional scale. *Scientific Reports*, *11*(1), Article 8293. https://doi.org/10.1038/s41598-021-86862-3

van Genuchten, M. Th. (1980). A closed-form equation for predicting the hydraulic conductivity of unsaturated soils. *Soil Science Society of America Journal*, *44*(5), 892–898. https://doi.org/10.2136/sssaj1980.03615995004400050002x

Whalley, W. R., Dumitru, E., & Dexter, A. R. (1995). Biological effects of soil compaction. *Soil and Tillage Research*, *35*(1–2), 53–68. https://doi.org/10.1016/0167-1987(95)00473-6

SUPPORTING INFORMATION

Additional supporting information can be found online in the Supporting Information section at the end of this article.

How to cite this article: Peters, A., Tian, Z., Heitman, J. L., Iden, S. C., Rolfes, L., Germer, K., & Lorenz, M. (2025). Modeling compaction effects on soil water retention across the full moisture range: Calibration and validation. *Vadose Zone Journal*, *24*, e70004. https://doi.org/10.1002/vzj2.70004

APPENDIX

A1 PDI model system

In the PDI system, the soil water retention function is given by Iden and Durner (2014):

$$\theta(h) = \left(\theta_s - \theta_r\right) S_c + \theta_r S_{nc}, \tag{A1}$$

where θ (-) is the volumetric water content, h (cm) is the suction, θ_s (-) is the saturated water content, θ_r (-) is the maximum content of noncapillary water, S_c (-) is the capillary saturation function, and S_{nc} (-) is the noncapillary saturation function. The first summand is the capillary water content, θ_c (-), and the second summand is the noncapillary water content, θ_{nc} (-).

To guarantee that the capillary saturation reaches zero at the suction at oven dryness, $h_0 = 10^{6.8}$ cm, the capillary saturation function is scaled by Iden and Durner (2014):

$$S_c(h) = \frac{\Gamma(h) - \Gamma\left(h_0\right)}{1 - \Gamma\left(h_0\right)}, \tag{A2}$$

where $\Gamma(h)$ is a basic saturation function, which can represent any uni- or multi-modal pore-size distribution. In our study, we restrict the analysis to the constrained van Genuchten (1980) saturation function:

$$\Gamma(h) = \left(\frac{1}{1 + (\alpha h)^n}\right)^{1-1/n} \tag{A3}$$

where α (cm^{-1}) and n (-) are shape parameters.

The noncapillary saturation function is given by Iden and Durner (2014):

$$S_{nc}(h) = \frac{\log\left(\frac{h_0}{h}\right) - \log(10)\, b \log\left(1 + \left[\frac{h_a}{h}\right]^{\frac{1}{\log(10) b}}\right)}{\log\left(\frac{h_0}{h_a}\right)}, \tag{A4}$$

where h_a (cm) is the suction head where noncapillary water reaches its saturation, and b (-) is a smoothing parameter, set to 0.2 (Peters et al., 2024). We define h_a as the suction at which the capillary saturation function, $S_c(h)$, reaches the upper quartile, resulting in (Peters, Hohenbrink, et al., 2023):

$$h_a = \alpha^{-1}\left(\gamma^{\frac{-1}{m}} - 1\right)^{1/n}, \tag{A5}$$

with

$$\gamma = 0.75\left(1 - \Gamma_0\right) + \Gamma_0, \tag{A6}$$

The PDI-vG model has 4 unknown parameters, namely, θ_s, θ_r, α, and n. The left panel of Figure A1 schemati-

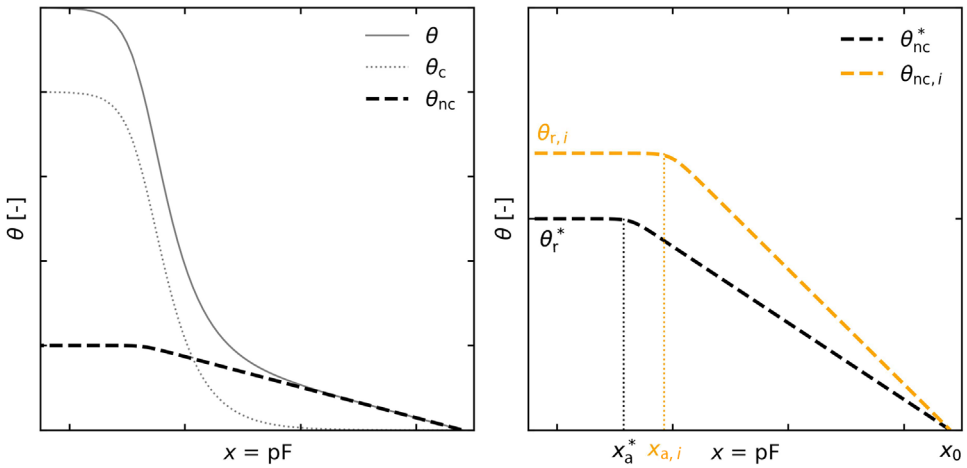

FIGURE A1 Left: Schematic representation of the Peters–Durner–Iden-van Genuchten (PDI-vG) water retention function. Right: Scaling of the noncapillary (adsorptive) component. θ, θ_c, and θ_{nc} are the total, the capillary, and the noncapillary volumetric water contents, x_a^* and $x_{a,i}$ indicate the pF values at the air-entry of the noncapillary part for the reference and the scaled curves, respectively, and x_0 is the pF value at oven dryness.

cally illustrates the PDI-vG water retention function and its components.

A2 Scaling of θ_r

As outlined by Peters et al. (2025), scaling θ_r within the PDI system is not possible in a similar way as presented in Tian et al. (2018) or Assouline (2006a), because the meaning of θ_r within the PDI is different from the traditional concept of a "residual water content." Peters et al. (2025) proposed a consistent scaling approach for θ_r within the PDI system, which is described in the following.

In the dry range, the noncapillary volumetric water content, θ_{nc} (-), is described as a linear function with respect to the log of suction and is zero at h_0 and reaches unity at h_a (see Figure A1, left). Therefore, it can be approximated as:

$$\theta_{nc} = \theta_r \frac{x_0 - x}{x_0 - x_a} \tag{A7}$$

where x, x_0, and x_a are the common logarithms of h, h_0, and h_a (see Equations A2–A6), that is, $x \equiv \text{pF}$. By assuming that the gravimetric noncapillary (i.e., adsorptive) water content is invariant with bulk density, the noncapillary water content of a soil with modified bulk density is calculated from the water content at reference bulk density (Figure A1, right):

$$\theta_{nc,i}(x) = \theta^*_{nc}(x) \frac{\rho_{b,i}}{\rho^*_b} = \theta^*_r \frac{x_0 - x}{x_0 - x^*_a} \frac{\rho_{b,i}}{\rho^*_b} \tag{A8}$$

Formulating Equation (A7) for the compacted case and inserting it into Equation (A8) gives:

$$\theta_{r,i} \frac{x_0 - x}{x_0 - x_{a,i}} = \theta^*_r \frac{x_0 - x}{x_0 - x^*_a} \frac{\rho_{b,i}}{\rho^*_b} \tag{A9}$$

Solving with respect to $\theta_{r,i}$ finally yields:

$$\theta_{r,i} = \theta^*_r \frac{x_0 - x_{a,i}}{x_0 - x^*_a} \frac{\rho_{b,i}}{\rho^*_b} \tag{A10}$$

Equation (A10) accounts for the shift in the retention curve caused by scaling the location parameter α, which changes x_a (see Equation A5) in the noncapillary saturation function. Therefore, x_a and x_a^* are not identical.

A3 Additional results

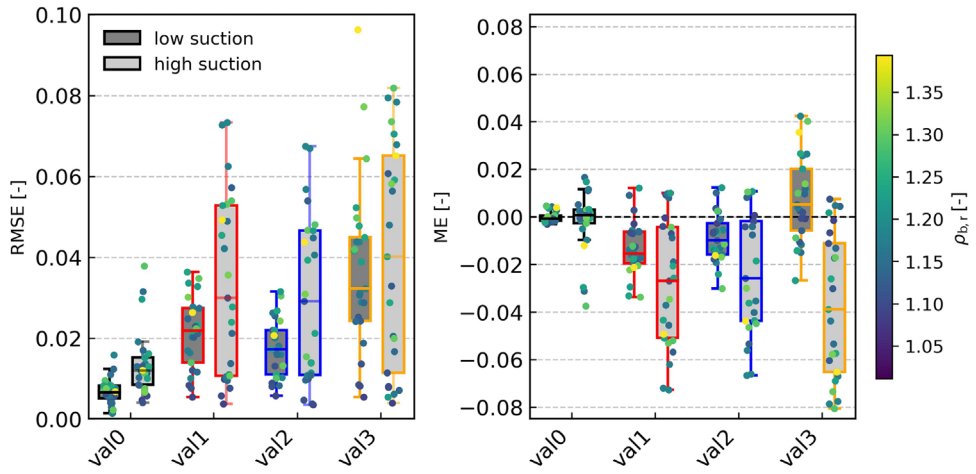

FIGURE A2 Boxplots for root mean square error (RMSE) and mean error (ME) for all validation variants (Table 3), differentiated between low suction data ($h < 1000$ cm) and high suction data ($h \geq 1000$ cm). val0: all parameters fitted, val1: all parameters predicted; val2: α, θ_r, and θ_s predicted, and n fixed; val3: all parameters are fixed to the reference values. The colors indicate the relative bulk density, $\rho_{b,r}$, given by the quotient of the bulk densities of the compacted soil and the reference.

TABLE A1 Statistical measures for the calibration data. The measures for the references are given in bold. The means and medians are calculated excluding the reference values. Numbers in brackets in first column indicate contents of sand, silt, and clay.

		cal1			cal2		
ID (texture)	**ρ_b (g cm^{-3})**	**RMSE (-)**	**ME (-)**	**R^2 (-)**	**RMSE (-)**	**ME (-)**	**R^2 (-)**
1 (0.90, 0.06, 0.04)	**1.50**	**0.0079**	**−0.00028**	**0.994**	**0.0079**	**−0.00028**	**0.994**
	1.52	0.0137	−0.00016	0.991	0.0165	0.00088	0.987
	1.53	0.0111	−0.00281	0.993	0.0123	−0.00153	0.993
	1.56	0.0094	0.00189	0.996	0.0109	0.00198	0.994
2 (0.54, 0.35, 0.11)	**1.22**	**0.0097**	**−0.00157**	**0.996**	**0.0097**	**−0.00157**	**0.996**
	1.28	0.0120	0.00103	0.994	0.0123	0.00144	0.994
	1.34	0.0098	0.00396	0.996	0.0116	0.00445	0.996
	1.44	0.0045	0.00086	0.996	0.0127	−0.00148	0.969
3 (0.32, 0.53, 0.15)	**1.32**	**0.0107**	**−0.00152**	**0.994**	**0.0107**	**−0.00152**	**0.994**
	1.40	0.0093	−0.00002	0.995	0.0129	0.00161	0.994
	1.48	0.0160	0.00746	0.988	0.0251	0.00994	0.984
4 (0.48, 0.34, 0.18)	**0.99**	**0.0098**	**−0.00194**	**0.995**	**0.0098**	**−0.00193**	**0.995**
	1.18	0.0241	−0.01138	0.970	0.0276	−0.00763	0.962
	1.32	0.0238	−0.01113	0.943	0.0259	−0.00981	0.928
6 (0.87, 0.02, 0.11)	**1.26**	**0.0045**	**−0.00211**	**1.000**	**0.0045**	**−0.00211**	**1.000**
	1.41	0.0172	0.01047	0.987	0.0212	0.01302	1.000
7 (0.30, 0.10, 0.60)	**1.06**	**0.0233**	**−0.00596**	**0.958**	**0.0233**	**−0.00557**	**0.958**
	1.22	0.0348	−0.00450	0.822	0.0349	−0.00716	0.835
8 (0.71, 0.21, 0.09)	**0.68**	**0.0046**	**0.00010**	**0.999**	**0.0046**	**0.00016**	**0.999**
	0.89	0.0045	0.00202	0.999	0.0075	0.00266	0.995
Mean		0.0141	−0.00009	0.977	0.0171	0.00076	0.975
Median		0.0120	0.00086	0.994	0.0129	0.00144	0.994

TABLE A2 Modified Akaike information criterion (AICc) values for all fitted curves to the calibration data except for the reference curves. Numbers in brackets in first column indicate contents of sand, silt, and clay.

ID (texture)	ρ_b (g cm^{-3})	cal0	cal1	cal2
1 (0.90, 0.06, 0.04)	1.52	−60.63	−71.17	−71.36
	1.53	−51.03	−65.56	−67.66
	1.56	−68.53	−78.04	−78.77
2 (0.54, 0.35, 0.11)	1.28	−187.95	−189.97	−191.49
	1.34	−210.80	−199.01	−194.00
	1.44	−177.52	−168.29	−137.37
3 (0.32, 0.53, 0.15)	1.40	−138.59	−144.81	−136.97
	1.48	−137.26	−127.39	−115.61
4 (0.48, 0.34, 0.18)	1.18	−65.38	−68.79	−69.32
	1.32	−63.86	−69.02	−70.56
6 (0.87, 0.02, 0.11)	1.41	−106.55	−67.18	−66.83
7 (0.30, 0.10, 0.60)	1.22	−1.76	−32.29	−37.27
8 (0.71, 0.21, 0.09)	0.89	–[a]	−44.09	−45.55

[a]AICc could not be calculated since number of data is 5 and number of adjusted parameters is 4 (see Equation 5).

TABLE A3 Peters–Durner–Iden (PDI) retention parameters for variant cal2 of the calibration data. The parameters for the references are given in bold. Numbers in brackets in first column indicate contents of sand, silt and clay.

		PDI parameter values			
ID (texture)	ρ_b (g cm^{-3})	α (cm^{-1})[a]	n (-)[b]	θ_r (-)[c]	θ_s (-)[c]
1 (0.90, 0.06, 0.04)	**1.50**	**0.170**	**8.30**	**0.0522**	**0.446**
	1.52	0.147	8.30	0.0523	0.439
	1.53	0.156	8.30	0.0529	0.435
	1.56	0.150	8.30	0.0537	0.423
2 (0.54, 0.35, 0.11)	**1.22**	**0.024**	**5.05**	**0.1829**	**0.541**
	1.28	0.021	5.05	0.1897	0.519
	1.34	0.017	5.05	0.1955	0.496
	1.44	0.014	5.05	0.2059	0.458
3 (0.32, 0.53, 0.15)	**1.32**	**0.014**	**4.31**	**0.1692**	**0.492**
	1.40	0.012	4.31	0.1770	0.463
	1.48	0.011	4.31	0.1855	0.433
4 (0.48, 0.34, 0.18)	**0.99**	**0.038**	**1.92**	**0.3033**	**0.607**
	1.18	0.015	1.92	0.3354	0.537
	1.32	0.010	1.92	0.3626	0.486
6 (0.87, 0.02, 0.11)	**1.26**	**0.032**	**3.22**	**0.1347**	**0.525**
	1.41	0.026	3.22	0.1480	0.468
7 (0.30, 0.10, 0.60)	**1.06**	**0.159**	**1.36**	**0.3000**	**0.600**
	1.22	0.049	1.36	0.3150	0.540
8 (0.71, 0.21, 0.09)	**0.68**	**0.102**	**1.44**	**0.2620**	**0.718**
	0.89	0.033	1.44	0.3130	0.641

[a]Parameter fitted.
[b]Parameter fixed.
[c]Parameter predicted.

TABLE A4 Peters–Durner–Iden (PDI) retention parameters for variant val2 of the validation data. The parameters for the references are given in bold. Numbers in brackets in first column indicate contents of sand, silt, and clay.

ID (texture)	ρ_b (g cm^{-3})	α (cm^{-1})[a]	n (-)[b]	θ_r (-)[c]	θ_s (-)[c]
9 (0.53, 0.37, 0.10)	**1.75**	**0.0028**	**3.10**	**0.1658**	**0.338**
	1.77	0.0026	3.10	0.1669	0.331
	1.80	0.0025	3.10	0.1686	0.319
	1.82	0.0024	3.10	0.1697	0.312
10 (0.72, 0.18, 0.10)	**1.32**	**0.1383**	**1.40**	**0.2509**	**0.502**
	1.43	0.1007	1.40	0.2653	0.460
	1.58	0.0675	1.40	0.2841	0.404
	1.71	0.0492	1.40	0.2998	0.355
	1.84	0.0367	1.40	0.2903	0.306
11 (0.88, 0.05, 0.07)	**1.50**	**0.1443**	**1.39**	**0.2035**	**0.407**
	1.58	0.1168	1.39	0.2110	0.379
	1.67	0.0936	1.39	0.2193	0.347
13 (0.85, 0.09, 0.06)	**1.44**	**0.0280**	**2.57**	**0.0782**	**0.365**
	1.50	0.0238	2.57	0.0804	0.347
	1.55	0.0209	2.57	0.0822	0.332
	1.60	0.0184	2.57	0.0839	0.317
	1.70	0.0144	2.57	0.0874	0.287
14 (0.18, 0.57, 0.25)	**1.09**	**0.3092**	**1.44**	**0.2942**	**0.588**
	1.19	0.2176	1.44	0.3132	0.551
	1.29	0.1576	1.44	0.3315	0.513
	1.38	0.1206	1.44	0.3476	0.479
15a (0.24, 0.45, 0.31)	**1.38**	**0.0179**	**1.45**	**0.2246**	**0.449**
	1.56	0.0112	1.45	0.2420	0.389
	1.55	0.0110	1.45	0.2430	0.386
	1.57	0.0107	1.45	0.2439	0.382
15b (0.24, 0.45, 0.31)	**1.19**	**0.0979**	**1.38**	**0.2478**	**0.496**
	1.26	0.0778	1.38	0.2578	0.472
	1.43	0.0469	1.38	0.2809	0.414
	1.52	0.0368	1.38	0.2926	0.384
16 (0.14, 0.66, 0.20)	**1.22**	**0.0588**	**1.41**	**0.2446**	**0.520**
	1.32	0.0429	1.41	0.2580	0.483
	1.47	0.0278	1.41	0.2771	0.429
	1.56	0.0220	1.41	0.2881	0.396

[a]Parameter predicted based on calibration.
[b]Parameter fixed.
[c]Parameter predicted.